**Title:**

# A pathway coordinated by DELE1 relays mitochondrial stress to the cytosol

Authors: Evelyn Fessler[1], Eva-Maria Eckl[1], Sabine Schmitt[2], Igor Alves Mancilla[1], Matthias F. Meyer-Bender[1], Monika Hanf[1], Julia Philippou-Massier[1], Stefan Krebs[1], Hans Zischka[2,3], and Lucas T. Jae[1]

Affiliations:

[1]Gene Center and Department of Biochemistry, Ludwig-Maximilians-Universität München, Feodor-Lynen-Strasse 25, 81377, Munich, Germany.

[2]Institute of Toxicology and Environmental Hygiene, School of Medicine, Technical University Munich, 80802 Munich, Germany.

[3]Institute of Molecular Toxicology and Pharmacology, Helmholtz Zentrum München-German Research Center for Environmental Health, Ingolstädter Landstrasse 1, 85764 Neuherberg, Germany.

Correspondence and requests for materials should be addressed to L.T.J. (jae@genzentrum.lmu.de).

**Mitochondrial fidelity is tightly linked to overall cellular homeostasis and compromised in aging and various pathologies[1–3]. Mitochondrial malfunction needs to be relayed to the cytosol, where an integrated stress response (ISR) is triggered through phosphorylation of eukaryotic translation initiation factor 2α (EIF2α) in mammalian cells[4,5]. EIF2α phosphorylation is mediated by the four EIF2α kinases GCN2, HRI, PERK and PKR, which are activated following diverse types of cellular stress[6]. Importantly, the machinery that communicates mitochondrial perturbation to the ISR has remained elusive[1,2,7]. Here we combine genome engineering and haploid genetics to unbiasedly identify genes affecting the induction of the ISR core factor CHOP (C/EBP homologous protein). This reveals the mitochondrial protease OMA1 and poorly-characterized protein DELE1, alongside HRI as the missing pathway triggered by mitochondrial insults. Mechanistically, stress-induced activation of OMA1 causes cleavage of DELE1 into a short form which accumulates in the cytosol, where it binds and activates HRI via its C-terminal portion. Obstruction of this pathway can be beneficial or adverse, depending on the type of mitochondrial perturbation. Beyond the core pathway components, our comparative genetic screening strategy points out a suite of auxiliary regulators, which together may inform future strategies to modulate the cellular response to mitochondrial dysfunction in human disease.**

Despite their partial autarky, mitochondria do not encode stress-response genes[1]. Instead, the ISR core component CHOP is among the most strongly induced factors in cells challenged with inhibition of the mitochondrial matrix chaperone TRAP1 by GTPP (gamitrinib-triphenylphosphonium) or the mitochondrial protease LON by CDDO (2-cyano-3,12-dioxo-oleana-1,9(11)-dien-28-oic acid)[7]. Because of their respective roles in protein folding and removal, inhibition of either factor causes protein misfolding in the mitochondrial matrix. CHOP is a transcription factor that can initiate apoptotic and non-apoptotic programs with a surprising ability to tune the response to different cellular cues[8]. The CHOP-encoding *DDIT3* gene is itself a target of the ISR transcription factor ATF4[1,7]. Additionally, it underlies translational regulation by an upstream open reading frame (uORF) that inhibits CHOP synthesis under basal conditions. While Ser51 phosphorylation of EIF2α reduces protein synthesis globally, it stimulates translation of CHOP, overriding the inhibitory effect of the uORF[2,8].

## Genome-wide perturbation screens

Whereas tunicamycin (TM), CDDO and the mitochondrial ionophore CCCP (carbonyl cyanide-*m*-chlorophenyl hydrazone) did not trigger profound changes in the abundance of heat shock protein HSPD1, they all led to a strong induction of CHOP in HAP1 cells (Extended Data Fig. 1a-b). To accurately capture CHOP protein production, we generated an endogenous fusion with mNeon at the *DDIT3* locus of HAP1 cells. A clonal population of such engineered cells responded to a challenge with CCCP, CDDO or TM by induction of $CHOP^{Neon}$ (Extended Data Fig. 1c-d). After subjecting haploid $CHOP^{Neon}$ cells to random genome mutagenesis by gene-trap, we challenged them with CCCP and sequenced mutations in cell populations showing a diminished or enhanced induction of $CHOP^{Neon}$ (Extended Data Fig. 1e)[9]. Gratifyingly, mutants defective in CHOP itself or its upstream transcriptional inducer ATF4 were strongly enriched among cells that poorly induced $CHOP^{Neon}$, alongside a wealth of additional regulators (Fig. 1a, Supplementary Table 1). To untangle general CHOP regulators from context-specific factors, we performed two additional orthogonal genome-wide screens using TM or CDDO (Fig. 1b, Extended Data Fig. 1f, Supplementary Tables 2-3). In line with its inhibitory effect on N-glycosylation[10], TM treatment highlighted numerous ER protein maturation and quality control genes, alongside its canonical EIF2α kinase

PERK[1,2]. By contrast, the effects of CDDO on CHOP were not blunted by any individual EIF2α kinase deficiency (Extended Data Fig. 1g)[7], possibly owing to the limited specificity of related compounds[11]. The comparative interrogation of CHOP regulators following three distinct cellular insults allowed us to differentiate global regulators of CHOP biology (Extended Data Fig. 1h-m) from such selectively operating in the context of CCCP-induced mitochondrial depolarization (Extended Data Figs. 2-4). In particular, stringent filtering for genes that prominently scored with CCCP, but not TM or CDDO, highlighted the transcriptional regulators TAF4 and GABPB1, glycolysis factors SLC2A1 and TPI1, and RNA binding proteins RBM27 and CLUH (*KIAA0664*). Moreover, the signature contained the mitochondrial proteins ATP5IF1 (*ATPIF1*) and OMA1. Most strikingly, it revealed a strong requirement for HRI (*EIF2AK1*) and the scarcely studied protein DELE1 (*KIAA0141*) (Fig. 1a, Extended Data Fig. 5a-b).

**Cellular dynamics of DELE1**

Given the scant knowledge on DELE1 and the unexpected involvement of HRI, we first sought to validate their requirement in a panel of cell systems including non-transformed cells, and indeed could confirm their importance in all cases (Extended Data Fig. 5c). Furthermore, CHOP induction also depended on DELE1 and HRI for other types of mitochondrial stress, including inhibition of complex V (oligomycin), TRAP1 (GTPP), and genetic ablation of LONP1 (Extended Data Fig. 5d-f). Failure to induce CHOP after stimulation with CCCP was preceded by a defect in EIF2α phosphorylation in HRI- or DELE1-deficient cells, suggesting that like HRI, DELE1 operates upstream of this event (Extended Data Fig. 5g). Strikingly, expression of HRI in DELE1 knockout cells was able to partially restore CHOP induction, whereas DELE1 expression in HRI-deficient cells was unproductive (Fig. 2a, Extended Data Fig. 6a-b). This indicated that DELE1 requires HRI to trigger CHOP but not vice versa, suggesting that DELE1 may act upstream of both EIF2α and HRI. Given that DELE1 is a mitochondrial protein[12] (Extended Data Fig. 6c), whereas HRI resides in the cytoplasm, we next wondered whether the activity of DELE1 towards HRI might be regulated by its localization. To test this hypothesis, we investigated if artificially re-routing DELE1 to the cytosol would bypass the need for a mitochondrial insult to provoke CHOP expression. Indeed, expression of a DELE1 mutant lacking the mitochondrial targeting sequence (DELE1$^{\Delta MTS}$) yielded a predominantly cytoplasmic protein that readily induced CHOP expression independently of CCCP (Fig. 2b-c, Extended Data Fig. 6d-e). This constitutively active version of DELE1 still required HRI to induce CHOP, underscoring its likely role as an activator of HRI.

Based on these findings, we asked whether the activity of wild-type DELE1 might be regulated via a similar mechanism. Indeed, while DELE1 localized to mitochondria in unperturbed cells, it could be detected in the cytosol upon CCCP treatment (Fig. 2d). We did not observe this behavior for MFN2, a mitochondrial protein affected by CCCP on similar time scales[13]. The redistribution of DELE1 to the cytosol was rapid and still occurred when de-novo protein synthesis was blocked, suggesting that it is mediated by a posttranslational event (Extended Data Fig. 6f). Indeed, time-resolved immunoblotting of exogenously expressed or endogenously tagged DELE1 after CCCP treatment revealed a reduction in molecular weight that coincided with its cytosolic accumulation and was preserved in the absence of HRI (Fig. 2e, Extended Data Fig. 6g-h). It could also be observed across different types of mitochondrial insults and cell systems, including primary cells, reinforcing the notion that DELE1 size reduction and localization are fundamentally entangled with its cellular function (Fig. 2f, Extended Data Fig. 6i-o).

**OMA1-mediated processing**

Our comparative genetic screens also exposed a role for the inner mitochondrial membrane (IMM) metallopeptidase OMA1 in CCCP-triggered CHOP expression, not shared with the TM and CDDO datasets (Fig. 1, Extended Data Fig. 7a). While OMA1 is mostly dormant in unstressed cells, its activity can be sparked by various mitochondrial homeostatic insults, leading to processing of the IMM fusion factor OPA1 and culminating in its own destruction[14] (Fig. 2f). As the precise triggers and substrate-specificity of OMA1 are incompletely understood, we wondered whether DELE1 might be a client of stress-activated OMA1. Whereas wild-type cells readily generated the short version of DELE1 (S-DELE1) following CCCP treatment, this processing was virtually blocked in OMA1 knockout cells or cells expressing the catalytic dead variant E328Q[15] and it was reduced by pharmacological inhibition of metallopeptidases but not other classes of proteases (Fig. 2g, Extended Data Fig. 7b-e)[14]. This prompted us to investigate whether OMA1-mediated cleavage of DELE1 would have an effect on its subcellular redistribution. Indeed, we observed that cytosolic localization of DELE1 upon exposure to CCCP was diminished in OMA1 knockout cells and cells expressing catalytic dead OMA1, but could be restored by $OMA1^{WT}$ (Fig. 2h). Cleavage of wild-type DELE1 also occurred in an OMA1-dependent fashion in isolated mitochondria depolarized *in organello*, and S-DELE1 was detectable in the mitochondrial supernatant (Extended Data Fig. 7f-k). Interestingly, while CCCP treatment led to processing of DELE1 and OPA1 on similar time scales, DELE1 cleavage and cytosolic accumulation occurred regardless of OPA1 status (Extended Data Fig. 8a-f).

**Interaction with HRI**

How would S-DELE1 in the cytosol lead to activation of HRI? Given that processed DELE1 should mostly consist of TPR domains, which mediate protein-protein interactions[16], we speculated that it may activate HRI via physical association. To test this, we co-expressed HRI with $DELE1^{\Delta MTS}$ or full-length DELE1 ($DELE1^{FL}$), subjected cells to CCCP treatment and precipitated HRI-bound proteins. This showed that $DELE1^{\Delta MTS}$ engaged in a constitutive interaction with HRI, whereas $DELE1^{FL}$ was only efficiently co-precipitated following its conversion into S-DELE1 (Extended Data Fig. 9a). Importantly, the same behavior was observed for the endogenous proteins (Fig. 3a). Stimulation of this pathway by CCCP or expression of $DELE1^{\Delta MTS}$ was accompanied by an electromobility shift of endogenous and exogenous HRI, indicative of activating autophosphorylation events[17] (Fig. 3b, Extended Data Fig. 9b-d). In agreement with the OMA1-dependent generation of S-DELE1, OMA1-deficient cells showed a reduction in the ability of HRI to precipitate wild-type DELE1 following CCCP exposure, whereas binding of $DELE1^{\Delta MTS}$ was unaffected (Extended Data Fig. 9e-f). Given the likely involvement of the DELE1 TPR domains, we next subjected this part of the protein to mutagenesis. Internal deletion mutations mapping to the upstream or downstream portion of the TPR-containing segment[12] localized to mitochondria in unstressed cells, got cleaved and accumulated in the cytosol after CCCP treatment (Extended Data Fig. 9g-h). While the corresponding ΔMTS mutants recapitulated the constitutive cytosolic localization of $DELE1^{\Delta MTS}$, they failed to co-precipitate HRI at detectable levels and did not (Δ246-272) or only minimally (Δ386-420) induce CHOP (Extended Data Fig. 9i-l). Conversely, a C-terminal fragment encompassing TPR domains 1-7 ($DELE1^{TPR1-7}$) was sufficient for HRI binding and CHOP induction (Extended Data Fig. 9m-n). Following stringent purification from sgHRI-treated cells, this fragment was also able to efficiently interact with HRI generated in *E.coli* (Fig. 3c, Extended Data Fig. 9o). The C-terminal removal of TPR domains from $DELE1^{TPR1-7}$ was better tolerated than removal from the N-terminus with respect to HRI co-precipitation and CHOP activation, with the exception of the first TPR domain, whose absence was compatible with HRI binding but not CHOP induction. As HRI is known to

respond to alterations in cellular heme[17], we tested whether heme would interfere with its ability to bind DELE1, which we did not observe (Extended Data Fig. 10a-c). Thus, OMA1-activated DELE1 is redistributed to the cytosol, where it interacts with HRI via its TPR domains to induce CHOP.

## Conclusion

Here, we uncover a proteolytic signaling axis involving OMA1, DELE1 and HRI that constitutes a long-sought link between mitochondrial perturbation and the cytosolic ISR (Extended Data Fig. 10d). Several of the insults routed through DELE1 perturb the mitochondrial membrane potential ΔΨ, which is known to trigger OMA1[14,15] and may explain the impact of ATP5IF1 and SLC2A1 on this pathway (Fig. 1a, Extended Data Fig. 10e-h): ATP5IF1 counteracts reversed activity of complex V when membrane potential is lost[18], thus aggravating CCCP-induced depolarization, while SLC2A1 is downregulated in low-ΔΨ cells[19]. Loss of ΔΨ depletes mitochondrial ATP[14,20], in line with our observation that DELE1 cleavage was also triggered by respiratory chain inhibitors. The ability of cells to cope with mitochondrial perturbation has an important impact on lifespan in model organisms and likely contributes to related phenotypes and age-associated diseases in humans[1–3,21]. Modulation of the ISR may be a promising strategy to interfere with dysfunctional mitochondria but could be complicated by its highly connected nature. Using transcriptomic profiling, we found that the cellular response to mitochondrial depolarization was severely blunted in DELE1- or HRI-deficient cells, resembling the effects of the ISR inhibitor ISRIB[22] (Fig. 3d-f), which blocks the impact of EIF2α phosphorylation and thus lacks selectivity for mitochondrial distress signaling. Intriguingly, in DELE1 or HRI knockout mutants and ISRIB-treated cells, CCCP caused a steep upregulation of heat shock proteins (including HSPA1A/B and DNAJB1), possibly reflecting an alternative program engaged by cells unable to signal through DELE1-HRI-EIF2α (Fig. 3e, Extended Data Fig 10i). Altered signaling was also mirrored by an increased resilience of cells defective for this pathway or treated with ISRIB in the face of mitochondrial depolarization (Fig. 3g, Extended Data Fig. 11a-c), without signs of generally altered mitochondrial physiology (Extended Data Fig. 11d-j). Conversely, cells deficient for DELE1 or HRI exhibited a subpar toleration of continuous mild mitochondrial perturbation elicited by a genetic deficiency in MFN2, suggesting a protective function in this context (Extended Data Fig. 11k-l). MFN2 plays a central role in mitochondrial dynamics and mitophagy and can cause peripheral neuropathies[13,23]. Of note, the exposed DELE1 biology was also operational in cells of neuronal origin (Extended Data Fig. 11m-o). Thus, manipulation of the OMA1-DELE1-HRI axis or auxiliary pathway components identified here may be beneficial under certain settings of mitochondrial malfunction in the context of human health.

**References:**


1. Higuchi-Sanabria, R. *et al.* A Futile Battle? Protein Quality Control and the Stress of Aging. *Dev. Cell* **44**, 139–163 (2018).
2. Shpilka, T. & Haynes, C. M. M. The mitochondrial UPR: Mechanisms, physiological functions and implications in ageing. *Nat. Rev. Mol. Cell Biol* **19**, 109–120 (2018).
3. Sun, N., Youle, R. J. & Finkel, T. The Mitochondrial Basis of Aging. *Mol. Cell* **61**, 654–666 (2016).
4. Quirós, P. M. *et al.* Multi-omics analysis identifies ATF4 as a key regulator of the mitochondrial stress response in mammals. *J. Cell Biol.* **216**, 2027–2045 (2017).
5. Harding, H. P. *et al.* An Integrated Stress Response Regulates Amino Acid Metabolism and Resistance to Oxidative Stress. *Mol. Cell* **11**, 619–633 (2003).
6. Taniuchi, S., Miyake, M., Tsugawa, K., Oyadomari, M. & Oyadomari, S. Integrated stress response of vertebrates is regulated by four eIF2α kinases. *Sci. Rep.* **6**, (2016).
7. Münch, C. & Harper, J. W. Mitochondrial unfolded protein response controls matrix pre-RNA processing and translation. *Nature* **534**, 710–713 (2016).
8. Palam, L. R., Baird, T. D. & Wek, R. C. Phosphorylation of eIF2 facilitates ribosomal bypass of an inhibitory upstream ORF to enhance CHOP translation. *J. Biol. Chem.* **286**, 10939–10949 (2011).
9. Brockmann, M. *et al.* Genetic wiring maps of single-cell protein states reveal an off-switch for GPCR signalling. *Nature* **546**, 307–311 (2017).
10. Azim, M. & Surani, H. Glycoprotein synthesis and inhibition of glycosylation by tunicamycin in preimplantation mouse embryos: Compaction and trophoblast adhesion. *Cell* **18**, 217–227 (1979).
11. Yore, M. M., Kettenbach, A. N., Sporn, M. B., Gerber, S. A. & Liby, K. T. Proteomic Analysis Shows Synthetic Oleanane Triterpenoid Binds to mTOR. *PLoS One* **6**, e22862 (2011).
12. Harada, T., Iwai, A. & Miyazaki, T. Identification of DELE, a novel DAP3-binding protein which is crucial for death receptor-mediated apoptosis induction. *Apoptosis* **15**, 1247–1255 (2010).
13. Tanaka, A. *et al.* Proteasome and p97 mediate mitophagy and degradation of mitofusins induced by Parkin. *J. Cell Biol.* **191**, 1367–1380 (2010).
14. Baker, M. J. *et al.* Stress-induced OMA1 activation and autocatalytic turnover regulate OPA1-dependent mitochondrial dynamics. *EMBO J.* **33**, 578–593 (2014).
15. Sekine, S. *et al.* Reciprocal Roles of Tom7 and OMA1 during Mitochondrial Import and Activation of PINK1. *Mol. Cell* **73**, 1028-1043.e5 (2019).
16. Scheufler, C. *et al.* Structure of TPR domain–peptide complexes: critical elements in the assembly of the Hsp70–Hsp90 multichaperone machine. *Cell* **101**, 199–210 (2000).
17. Lu, L., Han, A. & Chen, J.-J. J. Translation Initiation Control by Heme-Regulated Eukaryotic Initiation Factor 2alpha Kinase in Erythroid Cells under Cytoplasmic Stresses. *Mol. Cell. Biol.* **21**, 7971–7980 (2001).
18. Shah, D. I. *et al.* Mitochondrial Atpif1 regulates haem synthesis in developing erythroblasts. *Nature* **491**, 608–612 (2012).
19. Sukumar, M. *et al.* Mitochondrial Membrane Potential Identifies Cells with Enhanced Stemness for Cellular Therapy. *Cell Metab.* **23**, 63–76 (2016).
20. Baricault, L. *et al.* OPA1 cleavage depends on decreased mitochondrial ATP level and bivalent metals. *Exp. Cell Res.* **313**, 3800–3808 (2007).
21. Sorrentino, V. *et al.* Enhancing mitochondrial proteostasis reduces amyloid-β proteotoxicity. *Nature* **552**, 187–193 (2017).
22. Sidrauski, C. *et al.* Pharmacological brake-release of mRNA translation enhances cognitive memory. *Elife* **2**, e00498 (2013).
23. Züchner, S. *et al.* Mutations in the mitochondrial GTPase mitofusin 2 cause Charcot-

271 Marie-Tooth neuropathy type 2A. *Nat. Genet.* **36**, 449–451 (2004).
272
273
274
275

**Figure Legends:**

**Figure 1| Genome-wide perturbation profiling reveals regulators of CHOP in the context of different ISR triggers. a, b,** Genetic screen showing positive and negative regulators of $CHOP^{Neon}$ in cells treated with CCCP (**a**) or TM (**b**). Per gene (dots), the ratio of the mutation frequency in $CHOP^{Neon}$-high cells versus $CHOP^{Neon}$-low cells (y-axis) is plotted against the combined number of unique mutations identified in both populations (x-axis). n = $2.12 \times 10^7$ (**a**) or $2.07 \times 10^7$ (**b**) interrogated single cells. Genes enriched for mutations are dark grey (two-sided Fisher's exact test, FDR-corrected *P*-value ($P_{adj}$) < 0.05). Red dots specify genes that are highly significant in the CCCP but not TM or CDDO dataset.

**Figure 2| DELE1 operates upstream of HRI and accumulates in the cytosol after OMA1-mediated cleavage. a-b,** HAP1 $CHOP^{Neon}$ cells of the specified genotypes transiently transfected with the indicated cDNAs or empty vector (EV) were treated for 9 h with CCCP or DMSO and analyzed by flow cytometry. Per genotype $CHOP^{Neon}$ fluorescence intensity was normalized to EV + DMSO and compared with EV for each treatment (mean ± s.d. of n=3 independent biological samples; two-way ANOVA with Tukey's multiple comparisons correction; one representative of 6 independent experiments). **c,** DELE1 domain architecture. **d,** Confocal microscopy of DELE1-Flag-mNeon (FmN) and MFN2-FmN expressed in HeLa cells. **e,** DELE1-HA (hemagglutinin) expressing cells subjected to time-resolved CCCP treatment prior to analysis of DELE1 cleavage by HA immunoblotting. **f,** Cells with endogenously HA-tagged *DELE1* stimulated as indicated and analyzed by immunoblotting. **g,** Wild-type cells and clonal OMA1 knockouts reconstituted with the specified cDNAs transfected with DELE1-HA, treated and assayed by immunoblotting. **h,** Wild-type and clonal OMA1 knockout HeLa cells transfected with the indicated cDNAs, treated and assayed by confocal microscopy. DAPI and wheat-germ agglutinin (WGA) visualize nuclei and cell membranes, respectively, TRAP1 staining identifies mitochondria. Scale bars, 10 µm.

**Figure 3| DELE1 binds HRI in the cytosol and a deficiency in this pathway mimics ISR inhibition and alters fitness in the context of mitochondrial stress. a**, Endogenous HRI was immobilized on beads and its ability to co-precipitate endogenous HA-tagged DELE1 was analyzed by immunoblotting. **b**, Electromobility shift of endogenously Flag-tagged HRI after the indicated treatments. **c**, EGFP or $DELE1^{TRP1\text{-}7}$-EGFP were stringently purified from sgHRI-treated 293T cells and incubated with GST (glutathione *S*-transferase)-HRI produced in *E.coli*. Interaction was assessed by Coomassie staining and immunoblotting. GST-HRI co-precipitation is accompanied by its depletion from the corresponding supernatant. **d**, Model of the pathway. **e**, Transcriptomic profiling of wild-type HAP1 cells +/- ISRIB and knockout mutants following treatment with CCCP for 12 h (n=4 biologically independent samples per group). Differentially expressed genes upon CCCP (DESeq2 two-tailed Wald test, $P_{adj} < 10^{-12}$; |log2 FC| > 1.5) were hierarchically clustered. ATF4/CHOP target genes are enriched among genes strongly induced in DELE1-HRI-eIF2α signaling proficient but not deficient cells (two-sided Fisher's exact test, $P_{adj} < 2 \times 10^{-19}$, green box), heat shock proteins are enriched in the cluster of genes induced in the opposite samples ($P_{adj} < 3 \times 10^{-7}$, red box). **f**, HAP1 $CHOP^{Neon}$ cells of the specified genotypes treated for 9 h and analyzed by flow cytometry. Per genotype $CHOP^{Neon}$ intensity was normalized to its DMSO control (dotted line; mean ± s.d. of n=3 independent experiments; two-way ANOVA with Tukey's multiple comparisons correction). **g**, Specified HAP1 cells treated for 48 h as indicated and survivors were stained with crystal violet (n=2 independent experiments).

## Materials and Methods:

### Cell lines and culture.

HAP1 cells were cultured in IMDM-medium (ThermoFisher Scientific) supplemented with 10% heat-inactivated fetal calf serum (FCS; ThermoFisher Scientific) and 1% penicillin–streptomycin–glutamine solution (ThermoFisher Scientific). HEK293T (293T), HeLa, and HCT116 cells were maintained in DMEM (ThermoFisher Scientific) containing the aforementioned supplements, as were BJEH and primary fibroblasts (kind gifts from T. Brummelkamp). SH-SY5Y cells were kindly gifted from V. Hornung and maintained in DMEM supplemented with 15% FCS, 1% penicillin–streptomycin–glutamine and 1 mM sodium pyruvate. N/TERT-1 keratinocytes[24] (a kind gift from J. Rheinwald) were maintained in a 1:1 mixture of DMEM and Ham's F12 (ThermoFisher Scientific) supplemented with 2 mM L-glutamine (ThermoFisher Scientific), 0.2 ng $ml^{-1}$ epidermal growth factor (EGF), 25 µg $ml^{-1}$ bovine pituitary extract (BPE; ThermoFisher Scientific), 0.4 mM $CaCl_2$ and 1% penicillin–streptomycin (ThermoFisher Scientific).

### Generation of endogenously tagged cell lines.

To generate HAP1 $CHOP^{Neon}$ cells, haploid HAP1 cells were transfected with a pX330 plasmid (Addgene #42230) encoding an sgRNA targeting the last codon of CHOP/*DDIT3*, alongside a donor vector containing a cassette consisting of a glycine/serine linker, 3xFlag, mNeon, polyA signal, pause site, hPGK promoter, puromycin N-acetyltransferase, polyA signal. This cassette was flanked upstream and downstream by a synthetic sgRNA recognition site[25]. Another pX330 plasmid encoding an sgRNA against these synthetic sgRNA recognition sites was included to release the knock-in cassette after uptake into the transfected cells. Transfected cells were expanded and subjected to puromycin selection (1µg $ml^{-1}$) to enrich for cells that integrated the cassette into the genome. Subsequently, single cell clones were derived and analyzed for the in-frame integration of the donor cassette into the *DDIT3* locus by PCR and Sanger sequencing. 293T $HRI^{Flag}$ cells were created analogously, except that the knock-in vector contained a 3xFlag tag, followed by CMV-driven puromycin N-acetyltransferase cassette, flanked on both sides by an sgRNA sequence derived from the *D. rerio tia1l* locus. $DELE1^{HA}$ 293T cells were generated similarly, except that the donor vector contained a glycine/serine linker and 3xHA tag, flanked on either side by the sgRNA recognition site and homology arms mapping to ca. 330bp upstream and downstream of the stop codon at the *DELE1* locus. The sgRNA recognition sequence near the *DELE1* stop codon was eliminated in the donor DNA sequence via synonymous mutations.

### Haploid genetic screen for identification of CHOP regulators.

Ultradeep genome-wide mutagenesis of haploid HAP1 cells was carried out as described before[9]. Briefly, an mCherry-containing variant of gene-trap retrovirus[26] was produced in 293T cells and harvested for the first time 48 h after transfection, followed by five additional harvests every 12 h. Retroviral particles were concentrated by ultracentrifugation at 22.800 r.p.m for 2 h at 4°C and stored at 4°C over night. To generate random genomic mutations via insertional mutagenesis by the gene-trap virus[27], haploid HAP1 $CHOP^{Neon}$ cells were plated at 15 million cells and transduced with concentrated viral particles 24 h after plating, followed by two additional transductions. The resulting library of mutants was expanded, frozen and used for genetic screens.

To identify CHOP regulators, mutagenized HAP1 $CHOP^{Neon}$ cells were plated at 20% confluence in a total of 20 T175 flasks (Sarstedt) and treated 48 h after plating for 16 h with 20 µM CCCP, or 9 h with 10 µM Tunicamycin, or 2.5 µM CDDO. Subsequently, cells were harvested using Trypsin-EDTA (0.25 %, Gibco), stopped with full medium and washed with PBS. Dissociated cells were passed through a 40 µm cell strainer (Greiner, 542040) prior to

fixation with one pellet volume of BD fix buffer I (BD Biosciences) for 10 min at 37°C. Fixation was stopped with PBS containing 1% FCS, cells were once more passed through a 40 µm cell strainer and counted. Approximately 1.5 x $10^9$ cells were permeabilized with one pellet volume of cold BD perm buffer III (BD Biosciences) for 30 min on ice. Permeabilization was stopped with PBS containing 1% FCS and cells were blocked at 100 million cells $ml^{-1}$ in PBS + 1% FCS + 3% BSA for 30 min at RT. The $CHOP^{Neon}$ protein was stained with the anti-mNeonGreen antibody (Chromotek 32f6-10) diluted 1:2,500 in PBS + 1% FCS + 1% BSA for 2.5 h at RT on a rotator, followed by three 15 min washing steps with PBS + 1% FCS at RT on a rotator. Subsequently, secondary antibody staining (anti-mouse-AF488 (Life Technologies) 1:500) was performed in PBS + 1% FCS + 1% BSA for 1 h at RT on a rotator protected from light. For a DNA counterstain, 4′,6-diamidino-2-phenylindole (DAPI, Sigma-Aldrich, D9542) was added to the secondary antibody dilution at a final concentration of 2.5 µg $ml^{-1}$. After three washing steps as above, cells were resuspended at 100 million cells $ml^{-1}$ in PBS + 1% FCS, stored at 4°C and sorted on a BD Fusion cell sorter (BD Biosciences) using a 70 µm nozzle. Staining specificity was determined using a secondary antibody only control. Haploid cells were identified based on DNA content in the DAPI channel and of those, approximately $10^7$ cells of the bottom 4% $CHOP^{Neon}$-low and top 4% $CHOP^{Neon}$-high cells were sorted into PBS + 10% FCS for isolation of genomic DNA.

**Insertion site mapping and analysis.**

Genomic DNA was extracted from the sorted cell populations using the QIAamp DNA Mini Kit (Qiagen, 51306). De-crosslinking was performed at 56°C overnight, and subsequent DNA extraction was performed following the manufacturer's instructions. Gene-trap insertion sites of $CHOP^{Neon}$-high and -low populations were recovered as described previously[9], except that the ssDNA linkers used in the ligation reaction and the primers for the final PCR step contained standard Illumina barcodes to allow for indexed deep sequencing using two index reads. Amplified libraries were sequenced on a HiSeq1500 (Illumina) with a read length of 50 nt (single-end mode). Demultiplexing of indexed sequencing reactions was performed allowing 1 mismatch. Reads were aligned to the human genome (hg19) and analyzed as described previously[9], except that removal of genomic regions assigned to overlapping genes and 3'untranslated regions was omitted. Instead, symbols of overlapping genes were concatenated. Briefly, Bowtie[28] was used to align demultiplexed reads to the human genome, allowing one mismatch, followed by mapping to the coordinates of Refseq protein-coding genes with intersectBED[29]. While insertional mutagenesis yields viral integrations in both orientations relative to the transcriptional direction of the affected genes, only integrations in the sense orientation were considered disruptive and used for downstream analysis. For the identification of regulators of $CHOP^{Neon}$, per gene the number of unique gene-trap insertion sites in the query gene vs. the whole sample was compared between the $CHOP^{Neon}$-high and $CHOP^{Neon}$-low cell populations using a two-sided Fisher's exact test and Benjamini-Hochberg false discovery rate correction. Data were plotted as the combined number of unique mutations identified in the $CHOP^{Neon}$-high and $CHOP^{Neon}$-low population (x-axis) vs. their mutation ratio (high/low) normalized by the respective sizes of the datasets (y-axis). Scatterplots were created using python framework Plotly Dash or GraphPad Prism. Venn diagrams were created by filtering the data with SQL commands and plotting it using the python library matplotlib.

**Generation of knockout cell lines.**

Targeted knockout cell lines were generated using the CRISPR/Cas9 system either by transient transfection or transduction. For the latter approach, 293T cells were transfected with the plasmid pL-CRISPR.EFS.tRFP (Addgene #57819) containing the sgRNA for a gene of interest, and the lentiviral packaging plasmids pMDLg/pRRE, pRSV-Rev and VSV.G.

Cells were transduced following standard procedures and RFP positive cells were sorted on a Sony SH800Z cell sorter. Alternatively, cells were transiently transfected using pX330 plasmids containing the sgRNA of interest along with vectors encoding either puromycin or blasticidin resistance to allow transient selection of transfected cells. For HAP1, 293T, and HeLa cells, clonal progeny was generated and verified by PCR and Sanger sequencing.

**Treatments, transfections, transductions and live stains.**

Cells were treated with carbonyl cyanide-*m*-chlorophenyl hydrazone (CCCP, Sigma-Aldrich, C2759, 20 μM unless stated otherwise), Bardoxolone (2-cyano-3,12-dioxo-oleana-1,9(11)-dien-28-oic acid, CDDO, MedChemExpress, HY-14909, 2.5 μM), tunicamycin (TM, MedChemExpress, HY-A0098, 10 μM), gamitrinib TPP hexafluorophosphate (GTPP, MedChemExpress, HY-102007A, 10 μM), oligomycin (OM, CST, 9996L, 10 or 25 μM), antimycin (AM, Sigma-Aldrich, A8674, 50 μM), valinomycin (VM, BioTechne, 3373, 0.5 μM), pepstatin A (Pepstat. A, Enzo, ALX-260-085-M005, 50 μM), 1,10-phenanthroline monohydrate (o-Phen., Sigma-Aldrich, P9375, 500 μM), E-64 (Sigma-Aldrich, E3132, 1 μM), E-64d (Enzo, BML-PI107-0001, 50 μM), zVAD (Z-VAD-FMK, PeptaNova, 3188-v, 20 μM), 3,4-dichloroisocoumarin (DCI, Sigma-Aldrich, D7910, 100 μM), Pefabloc® SC Plus (Sigma-Aldrich, 1187360100, 500 μM), ISRIB (Sigma-Aldrich, SML0843, 200 nM), hemin (Sigma-Aldrich, 51280, 20 μM) or cycloheximide (CHX, Sigma-Aldrich, C4859, 20 μg $ml^{-1}$) for the indicated times.

Where indicated, cells were transfected 24 to 36h before treatment using polyethylenimine (PEI 25000, Polysciences) or Turbofectin (OriGene Technologies). Transductions were performed as described previously[26].

Mitochondrial membrane potential was assessed using 100 nM tetramethylrhodamine (TMRM, ThermoFisher) following the manufacturer's instructions.

**Immunoprecipitation and immunoblotting.**

Cells for Western blot analysis were seeded and treated as described in the figure legends. To harvest cell lysates, cells were washed with PBS and lysed with RIPA or SDS sample buffer. After boiling the samples at 75-99 °C for 10 min, proteins were separated by gel electrophoresis using the Bolt gel electrophoresis system (ThermoFisher Scientific), following the manufacturer's instructions. 4-12% Bolt gradient gels were used for routine immunoblot analysis and for analysis of small molecular weight changes proteins were separated using 8% Novex gels. After transfer onto polyvinylidene fluoride (PVDF) membranes, proteins were detected with the indicated antibodies.

Cells for co-immunoprecipitation experiments were seeded in 10-cm dishes and treated as described in the figure legends. Cells were washed with cold PBS and lysed in DISC buffer (30 mM TRIS-HCl pH 7.5, 150 mM NaCl, 10% glycerol, 1% Triton X100) with freshly added protease inhibitor cocktail (cOmplete™ Protease Inhibitor Cocktail, Roche, 11697498001). Cell lysates were incubated on ice for 20 minutes and subsequently lysates were cleared twice by centrifugation at 20,000*g* for 15 minutes at 4°C. An aliquot of the supernatant was kept as input. The cleared supernatants were incubated with either Strep-Tactin Superflow Plus Beads (Qiagen, 30002) or Anti-FLAG M2 Magnetic Beads (Sigma, M8823) for precipitation of StrepTagII or Flag containing protein complexes, respectively. Beads were blocked with 3% BSA in PBS for 30 min at 4°C on a rotator and washed five times with DISC before addition of supernatants. For co-immunoprecipitation of proteins bound to endogenous HRI protein, cleared supernatants were incubated with the anti-EIF2AK1 antibody (Proteintech, 20499-1-AP) at a dilution of 1:1000 at 4°C on a rotator over night. Subsequently, Pierce™ Protein A agarose beads (ThermoFisher Scientific, 20334) were added to the lysates.

After a 2.5 h incubation at 4°C on a rotator, beads were washed five times 5 min each with DISC buffer. After the last washing step, DISC buffer was removed completely, SDS sample buffer was added, beads were boiled at 99 °C for 10 min and proteins were analyzed by Western blotting as described above.
For phosphatase treatment of protein lysates, cells were lysed in RIPA buffer (150 mM NaCl, 0.1% SDS, 50 mM TRIS-HCl pH 7.5, 1% TritonX100, 0.5% sodium deoxycholate) with freshly added protease inhibitor cocktail for 15 min on ice and lysates were cleared by centrifugation at 20,000*g* for 15 minutes at 4°C. Subsequently, 26 µl of supernatant were transferred to a microfuge tube, 4 µl 10x FastAP buffer and 10 µl FastAP Thermosensitive Alkaline Phosphatase (Thermo Fisher Scientific, EF0654) or RIPA in control samples were added. Samples were incubated at 37°C for 1 h and reaction was stopped by the addition of 4x SDS sample buffer. For gel source data, see Supplementary Figure 1.

**EGFP trap purification.**
For generation of DELE$^{TPR1-7}$-EGFP and EGFP control protein, sgHRI-treated 293T cells were transfected with plasmids expressing the respective transgenes from a CMV promoter and harvested 48 h post transfection. Briefly, after two washes with PBS, cells were scraped and snap-frozen in liquid $N_2$. Frozen pellets were then lysed in high salt lysis buffer (1 M KCl, 50 mM HEPES-KOH pH 7.2, 10% glycerol, 1% IGEPAL CA-630) supplemented with cOmplete™, Mini, EDTA-free Protease Inhibitor Cocktail (Roche, 11836170001). Lysates were sonicated and subjected to Pierce™ Universal Nuclease for Cell Lysis (ThermoFisher Scientific, 88700) treatment for 30 min at 4 °C to digest DNA. Lysates were cleared twice by centrifugation for 10 min at 21,000*g* after which input was set aside and the remaining lysates were incubated with 40 µl of GFP-TRAP® Magnetic Agarose beads (Chromotek, gtma-20) for 2 h at 4 °C. After immunoprecipitation, beads were washed three times with high salt buffer (0.5 M KCl, 50 mM HEPES-KOH pH 7.2, 10% glycerol), followed by three washes using DISC buffer. A fraction of bead-purified protein was put aside and the remaining beads were combined with 1.6 ug of recombinant GST-HRI protein produced in *E.coli* (Abnova, P5769) per reaction and incubated in DISC buffer at 4 °C over night. Subsequently, supernatant was collected and beads were washed six times with DISC buffer, prior to addition of sample buffer and analysis by SDS-PAGE, alongside immunoprecipitation supernatant and GST-HRI input (85% of IP was subjected to analysis by Coomassie stain, 5%, 2.5% and 1.25% of IP, supernatant and GST-HRI input, respectively, were used for immunoblot analysis). Cell lysate input was analyzed analogously pre and post exposure to GFP-TRAP® beads to assess purity. SDS gels were either stained for 1 h using InstantBlue™ Coomassie Protein Stain (Expedon, ISB1L) or subjected to immunoblotting. In the latter case, DELE$^{TPR1-7}$-EGFP and EGFP were detected using a rat anti-GFP antibody (Chromotek, 3h9) different from the alpaca nanobody conjugated to the GFP-TRAP® beads, whereas GST-HRI was detected using an antibody directed against GST (GE Healthcare, 27457701V).

**Crystal Violet staining.**
Cells for staining were seeded in 6-well or 96-well plates and treated as described in figure legends. Subsequently, cells were fixed by adding 3.7% PFA for 10 min, washed twice with PBS and stained with Crystal violet solution (12.25 mM crystal violet (Carl-Roth, T123.1), 20% methanol) for 20 seconds. Staining solution was washed off with water and plates were dried at RT.

**Analytical flow cytometry.**
For analysis of CHOP$^{Neon}$ fluorescence or mitochondrial membrane potential after treatment, cells were detached using Trypsin-EDTA (0.25 %, Gibco) and measured on a BD LSRFortessa flow cytometer (BD, Franklin Lakes, New Jersey, USA). Data were analyzed

using BD FACSDiva (BD, Franklin Lakes, New Jersey, USA) or FlowJo software (TreeStar Inc, Ashland, Oregon, USA).
For transient transfection of HAP1 CHOP$^{Neon}$ cells with cDNAs of interest, mCherry was co-transfected to identify transfected cells. Gating was performed as follows: To identify transfected cells, top 10% of mCherry positive cells were gated and their mean mNeon intensity was divided by the mean mNeon intensity of untransfected (mCherry-negative) cells. For analysis of genetic LONP1 ablation, CHOP$^{Neon}$ cells were seeded in 12-well plates and transduced with a lentiviral construct encoding TagRFP and an sgRNA targeting the indicated genes or a non-targeting control sgRNA. Cells were cultured for 9 days and CHOP$^{Neon}$ levels in TagRFP+ cells were analyzed by flow cytometry. For fitness assays, cells were seeded in triplicates into 12-well plates and separately infected with a lentiviral construct encoding TagRFP and an sgRNA targeting the indicated genes or a non-targeting control sgRNA. The percentage of TagRFP+ sgRNA-containing cells was followed over time and normalized to the non-targeting sgRNA control and day 0 measurements.

**Immunofluorescence.**
Cells were seeded at 20% confluence on poly-L-lysine-coated glass cover slips or in µ-Slide chambered coverslips (ibidi, 80826). 24 to 36 h after transfection, cells were pre-stained with 100 nM Mitotracker Red (Molecular Probes MitoTracker Red CMXRos, Thermo Fisher Scientific, M7512) for 1 h where indicated and subjected to drug treatments. Where indicated, cells were washed with PBS and stained with WGA647 (ThermoFisher Scientific, W32466) diluted 1:2000 in PBS for 5 min at RT. Cells were washed with PBS and fixed with 3.7% PFA for 10 min at RT. After fixation, cells were washed twice with PBS and permeabilized with 0.05% Triton-X 100 in PBS for 30 min at RT, washed twice with PBS and blocked in 10% normal goat serum (NGS, VWR, UPTIUP379030) in PBS for 30 min at RT. For visualization of the respective proteins, cells were incubated with primary antibodies in 10% NGS in PBS for at least 1 h at RT. After washing three times with PBS, fluorophore-conjugated secondary antibodies were diluted in 10% NGS in PBS and applied for 1 h at RT in the dark. Cells were washed three times with PBS (second wash containing 1 µg ml$^{-1}$ DAPI when required) and coverslips were mounted with Roti-Mount FluorCare (Carl Roth HP19.1). Imaging was performed with a Zeiss Observer.Z1 confocal microscope (Carl Zeiss, Oberkochen, Germany) equipped with an 63x oil immersion objective. Images were obtained using the ZEN 2009 software (Carl Zeiss, Oberkochen, Germany). Where indicated, imaging was performed with a Leica DMi8 light microscope (Leica, Wetzlar, Germany) and images were obtained using the LasX software (Leica, Wetzlar, Germany). All images were analyzed using Fiji[30].

**Isolation of mitochondria, *in vitro* FCCP treatment and electron microscopy.**
Mitochondria from 293T cells were isolated as previously described[31]. Briefly, cells from one 15-cm dish were resuspended in 1.0-1.5 ml isolation buffer (300 mM Sucrose, 5 mM TES, 200 µM EGTA, pH 7.2). 1 ml of this cell suspension was pumped three times through the cell homogenizer (6 µm clearance) with a constant rate of 1000 µl/min and subsequently transferred to a 2 ml microfuge tube. Thereafter 1 ml of isolation buffer was pumped one time (6 µm clearance, 1000 µl/min) through the cell homogenizer and transferred to the 2 ml tube. This procedure was repeated for the remaining cell suspension.
The homogenate was centrifuged at 800*g* for 5 min at 4°C, the supernatant was transferred to a fresh 2 ml microfuge tube and the pellets were resuspended in 150 µl 2x Lämmli buffer, frosted in liquid nitrogen and stored at -80°C for Immunoblot analysis. Subsequently, the supernatant was centrifuged at 10,000*g* for 10 min at 4°C. 150 µl of the supernatant were transferred to a 1.5 ml microfuge tube, mixed with 150 µl 2x Lämmli, frosted in liquid nitrogen and stored at -80°C for Immunoblot analysis. The rest of the supernatant was

discarded and the pellets (mitochondria) were resuspended in isolation buffer. Protein concentration was determined by the Bradford assay[32] and subsequently adjusted to 2 µg µl$^{-1}$ with isolation buffer. 30 to 120 µL of this suspension was used for *in vitro* FCCP treatment. The remaining mitochondria were centrifuged at 10,000*g* for 10 min at 4°C and resuspended in 2x Lämmli with a concentration of 2 µg µl$^{-1}$, frosted in liquid nitrogen and stored at -80°C for immunoblot analysis.

Mitochondrial transmembrane potential was determined as described previously[33]. The assay was performed in black 96 well plates and per well 30 µl of mitochondria (2 µg µl$^{-1}$) were either mixed with 50 µl of 500 nM rhodamine 123 (Invitrogen, R302), 50 µl 0.02% DMSO and 70 µl of swelling buffer (200 mM sucrose, 10 mM MOPS-Tris, 5 mM succinate (Merck, 8.20151.0100), 5 mM pyruvate (Sigma-Aldrich, P2256), 2 mM malate (Sigma-Aldrich, 02288), 1 mM $H_3PO_4$, and 10 µM EGTA) or with 50 µl 500 nM rhodamine 123, 50 µl 2µM FCCP (final concentration of 500 nM; in 0.02% DMSO; Sigma-Aldrich, C2920), and 70 µl of swelling buffer. Membrane potential was measured for 1 h at 37°C (excitation 495/15, emission 537/10) in a multiplate reader. Subsequently, 100 µl from each well were transferred to a 1.5 ml microfuge tube and centrifuged at 10,000*g* for 10 min at 4°C. The supernatant was transferred to a fresh 1.5 ml microfuge tube and mixed with an equal amount of 2x Lämmli. The pellet was resuspended in 15 µl 2x Lämmli. In case of replicates, the samples were pooled and the amount of added 2x Lämmli was adjusted accordingly. Samples were frosted in liquid nitrogen and stored at -80°C for immunoblot analysis.

Electron microscopy of isolated mitochondria was done as previously described[34]. Samples were fixed with 2.5% glutaraldehyde in 0.1 M sodium cacodylate buffer, pH 7.4 (Electron Microscopy Sciences, Hatfield, USA) for 24 h at the minimum. Thereafter glutaraldehyde was removed and samples were washed three times with 0.1 M sodium cacodylate buffer, pH 7.4. Postfixation and prestaining was done for 45 to 60 min with 1% osmium tetroxide (10 ml 4% osmium teroxide (Electron Microscopy Sciences, 19190), 10 ml dd$H_2O$, 10 ml 3.4% sodium chloride and 10 ml 4.46% potassium dichromate (pH adjusted to 7.2 with KOH (Sigma Aldrich)). Samples were washed three times with dd$H_2O$ and dehydrated with an ascending ethanol series (15 min with 30%, 50%, 70%, 90% and 96%, respectively, and three times 10 min with 100%) and propylene oxide (two times 30 min, Serva Electrophoresis GmbH, Heidelberg, Germany). Subsequently, samples were embedded in Epon (3.61 M glycidether 100 (Serva Electrophoresis GmbH), 1.83 M methylnadicanhydride (Serva Electrophoresis GmbH), 0.92 M dodecenylsuccinic anhydride (Serva Electrophoresis GmbH), 5.53 mM 2,4,6-tris(dimethylaminomethyl)phenol (Serva Electrophoresis GmbH)). Ultrathin sections were automatically stained with UranyLess EM Stain (Electron Microscopy Sciences) and 3% lead citrate (Leica, Wetzlar, Germany) using the contrasting system Leica EM AC20 (Leica, Wetzlar, Germany) and examined with an JEOL -1200 EXII transmission electron microscope (JEOL GmbH, Freising, Germany).

**Seahorse measurements.**

Mitochondrial function was assessed using the Agilent Seahorse XF Cell Mito Stress Test Kit and Seahorse XFe96 FluxPak (Agilent Technologies, 103015-100 and 102601-100), and the oxygen consumption rate was monitored with the Seahorse XFe96 Analyzer (Agilent Technologies) following the manufacturer's instructions. 2 x $10^4$ HeLa cells of the indicated genotypes were seeded in a 96-well plate on the day prior to the assay including four to six replicate culture wells per run. One hour before the assay, cells were washed twice with Seahorse XF DMEM medium (Agilent Technologies, 103575-100) followed by addition of 180 µl Seahorse XF DMEM medium per well, supplemented with 1 mM pyruvate, 2 mM glutamine and 10 mM glucose (Agilent Technologies, 103578-100, 103579-100 and 103577-

100). Subsequently, cells were placed in a $CO_2$-free BioTek Cytation 1 imaging reader, where bright field images of each well were taken. The Mito Stress Test was performed following the standard protocol. For oligomycin and Rot/AA the recommended concentrations of 1.5 µM and 0.5 µM, respectively, were used. The optimal FCCP concentration was determined by titration from 0.125 to 1 µM and was found to be 250 nM. To determine cell numbers, Hoechst 33342 (Thermo Fisher Scientific, 62249) was added to the Rot/AA dilution to reach a final concentration of 8 µM. After completion of the Mito Stress Test, cells were returned to the BioTek Cytation 1 imaging reader where fluorescence images of the Hoechst 33342 signal were taken. The resulting cell numbers were imported into the Wave 2.6.1 software and normalization was applied. The Seahorse XF Mito Stress Test Report Generator 4.03 was used for analysis.

**RNAseq.**

HAP1 wild-type and clonal knockout cells were plated on the day before treatment in 6-well plates. On the next day, cells were treated with CCCP and/or ISRIB as indicated for 12 h. Per condition, two independent clones were treated in two replicates each. Subsequently, cells were washed once with PBS and lysed in TRIzol™ reagent (Thermo Fisher Scientific, 15596018) on ice. Lysates were transferred to microfuge tubes, snap frozen in liquid nitrogen and stored at -80°C.

RNA of 300 µl TRIzol lysate was isolated using the Maxwell RSC miRNA Tissue Kit (Promega, AS1460) following manufacturer's instructions. Afterwards, RNA concentration was quantified (NanoDrop, ThermoFisher) and 1 µg of isolated RNA was additionally purified using Agencourt RNAClean XP Beads (Beckman Coulter, A63987). The purified RNA was quantified and quality controlled (Bioanalyzer, Agilent). For generating sequencing libraries 500 ng high quality RNA (RIN > 8.0) was processed using the SENSE mRNA-Seq Lib Prep Kit V2 (Lexogen, A01161). Sequencing was performed using a HiSeq1500 instrument (Illumina, San Diego, CA) with a read length of 50 nt, single-end mode. Transcriptome data was analyzed using the Galaxy web interface[35]. After demultiplexing and recommended trimming the data was mapped against the human genome (hg19) using RNA-STAR mapper (Galaxy version 2.5.2b-0). The abundance of mapped reads was analyzed using HTseq-count (Galaxy version 1.0.0). Afterwards, a differential gene expression analysis based on the negative binominal distribution was performed based on 4 replicates per condition (2 independent clones treated in duplicates) using DESeq2 (Galaxy version 2.11.39) setting the FDR < 0.05 (ref[36]). DESeq2 output is provided in Supplementary Tables 6-10.

For hierarchical clustering, genes with an FDR-adjusted *P*-value < $10^{-12}$ and a |log2 FC| > 1.5 in at least one of the datasets were considered. Clustering was performed using Cluster 3.0 (ref[37]), employing an uncentered correlation as distance measure and complete linkage clustering as clustering method. The results were visualized using Java TreeView Version 1.1.6r4 (ref[38]). A list of ATF4/CHOP targets was compiled by combining annotated ATF4 and CHOP target genes[39] with ATF4 binding site data[40]. Heat shock proteins were derived by gene ontology analysis[41–43]. Significant enrichment of gene collections (ATF4/CHOP target genes, and heat shock proteins) among clusters was calculated using a two-sided Fisher's exact test, followed by FDR-correction. Densities on the heatmap were defined as 2 divided by the sum of distances to the left and right neighbor (the distance of two directly adjacent genes being 1 unit). For genes at the edge, the distance to their only neighbor was doubled. Volcano plots were assembled using unfiltered DESeq2 output of the complete data and plotted using python framework Plotly Dash.

**Cloning of cDNAs.**

Coding sequences of genes expressed in this study were amplified from human cDNA, the coding sequence of MFN2 was amplified from MFN2-YFP (Addgene #28010). All primer

sequences are listed in Supplementary Table 4. Amplified DNA was subjected to restriction digest and ligation using standard cloning procedures. All cloned constructs were sequence-verified by Sanger sequencing.

**Statistics and reproducibility.**

For genome-wide genetic screens, $2.12 \times 10^7$ (CCCP), $2.07 \times 10^7$ (Tunicamycin) and $1.90 \times 10^7$ (CDDO) individual single cells were interrogated phenotypically by fluorescence and genetically by deep sequencing. This yielded a total of 5,579,161 unique sense mutations (averaging 297 unique mutations per identified gene) for the CCCP data, 4,883,298 (averaging 262 per gene) for the Tunicamycin data and 4,286,443 (averaging 232 per gene) for the CDDO data. Per experiment, a two-sided Fisher's exact test was employed to calculate enrichment of mutations in the high or low channel and *P*-values were false discovery rate (FDR)-corrected using the Benjamini-Hochberg method[9].

For analytical flow cytometry data, unless stated otherwise in the figure legend, data represent the mean ± s.d. of n=3 biologically independent experiments, each experiment containing triplicate specimen (i.e. separately cultured/treated cell populations). Statistical significance was assessed as described in the figure legends using GraphPad Prism 8.

For immunoblotting data, unless stated otherwise in the figure legend, data show a representative of n=3 biologically independent experiments with similar results. For quantification of immunoblot data statistical significance was assessed using GraphPad Prism 8 with the appropriate type of analysis (i.e. *t*-test for a single comparison and ANOVA for multiple comparisons) and false discovery correction, as indicated in the figure legends.

For microscopy experiments, unless stated otherwise in the figure legend, data indicate a representative of n=3 biologically independent experiments with similar results.

A detailed account of the processing and statistical analysis of RNAseq data is provided in the respective methods section.

**Data availability statement.**

All deep sequencing raw data (genome-wide genetic screens and RNAseq) have been deposited in the NCBI Sequence Read Archive under accession number PRJNA559719. The corresponding processed data are provided in the Supplementary Tables 1-3 and 6-10. All source data are provided with the paper. Any additional data, information, resources and reagents are available from the corresponding author upon reasonable request.

**References (continued):**


24. Dickson, M. A. *et al.* Human Keratinocytes That Express hTERT and Also Bypass a p16INK4a-Enforced Mechanism That Limits Life Span Become Immortal yet Retain Normal Growth and Differentiation Characteristics. *Mol. Cell. Biol.* **20**, 1436 LP – 1447 (2000).
25. Schmid-Burgk, J. L., Höning, K., Ebert, T. S. & Hornung, V. CRISPaint allows modular base-specific gene tagging using a ligase-4-dependent mechanism. *Nat. Commun.* **7**, 12338 (2016).
26. Jae, L. T. *et al.* Lassa virus entry requires a trigger-induced receptor switch. *Science (80-. ).* **344**, 1506–1510 (2014).
27. Carette, J. E. *et al.* Haploid genetic screens in human cells identify host factors used by pathogens. *Science (80-. ).* **326**, 1231–1235 (2009).
28. Langmead, B., Trapnell, C., Pop, M. & Salzberg, S. L. Ultrafast and memory-efficient alignment of short DNA sequences to the human genome. *Genome Biol.* **10**, R25 (2009).
29. Quinlan, A. R. & Hall, I. M. BEDTools: a flexible suite of utilities for comparing genomic features. *Bioinformatics* **26**, 841–842 (2010).
30. Schindelin, J. *et al.* Fiji: an open-source platform for biological-image analysis. *Nat. Methods* **9**, 676 (2012).
31. Schmitt, S. *et al.* A semi-automated method for isolating functionally intact mitochondria from cultured cells and tissue biopsies. *Anal. Biochem.* **443**, 66–74 (2013).
32. Bradford, M. M. A rapid and sensitive method for the quantitation of microgram quantities of protein utilizing the principle of protein-dye binding. *Anal. Biochem.* **72**, 248–254 (1976).
33. Zamzami, N., Métivier, D. & Kroemer, G. Quantitation of mitochondrial transmembrane potential in cells and in isolated mitochondria. *Methods Enzymol.* **322**, 208–213 (2000).
34. Zischka, H. *et al.* Electrophoretic Analysis of the Mitochondrial Outer Membrane Rupture Induced by Permeability Transition. *Anal. Chem.* **80**, 5051–5058 (2008).
35. Afgan, E. *et al.* The Galaxy platform for accessible, reproducible and collaborative biomedical analyses: 2018 update. *Nucleic Acids Res.* **46**, W537–W544 (2018).
36. Love, M. I., Huber, W. & Anders, S. Moderated estimation of fold change and dispersion for RNA-seq data with DESeq2. *Genome Biol.* **15**, 550 (2014).
37. de Hoon, M. J. L., Imoto, S., Nolan, J. & Miyano, S. Open source clustering software. *Bioinformatics* **20**, 1453–1454 (2004).
38. Saldanha, A. J. Java Treeview - Extensible visualization of microarray data. *Bioinformatics* **20**, 3246–3248 (2004).
39. Han, H. *et al.* TRRUST v2: An expanded reference database of human and mouse transcriptional regulatory interactions. *Nucleic Acids Res.* **46**, D380–D386 (2018).
40. Bao, X. R. *et al.* Mitochondrial dysfunction remodels one-carbon metabolism in human cells. *Elife* **5**, e10575 (2016).
41. Ashburner, M. *et al.* Gene ontology: tool for the unification of biology. The Gene Ontology Consortium. *Nat. Genet.* **25**, 25–29 (2000).
42. The Gene Ontology Consortium. The Gene Ontology Resource: 20 years and still GOing strong. *Nucleic Acids Res.* **47**, D330–D338 (2018).
43. Carbon, S. *et al.* AmiGO: online access to ontology and annotation data. *Bioinformatics* **25**, 288–289 (2008).
44. Quirós, P. M., Langer, T. & López-Otín, C. New roles for mitochondrial proteases in health, ageing and disease. *Nat. Rev. Mol. Cell Biol* **16**, 345–359 (2015).
45. Calvo, S. E., Clauser, K. R. & Mootha, V. K. MitoCarta2.0: An updated inventory of

769 mammalian mitochondrial proteins. *Nucleic Acids Res.* **44**, D1251–D1257 (2016).
770
771

**Acknowledgements:** We thank A. Graf and H. Blum for deep sequencing infrastructure, C. Jung for assistance with confocal microscopy, N. Tafrishi for assistance with cell sorting, and S. Theurich for access to Seahorse instrumentation. We thank T. Brummelkamp and V. Hornung for valuable comments on the manuscript, and J. Stingele, R. Beckmann, and all members of the Jae lab for helpful discussions. This work was supported by ERC StG 804182 - *SOLID*, the Center for Integrated Protein Science Munich, and the German Research Foundation (Heinz-Maier-Leibnitz Prize) to L.T.J.

**Author Contributions:** E.F. and L.T.J. conceived the study. E.F., E.E. and L.T.J. performed experiments and analyzed data. S.S. performed mitochondrial isolations and *in organello* stimulations. I.A.M. generated knockout cell lines. M.F.M-B. performed bioinformatics analyses. J.P-M. generated and analyzed RNAseq libraries, S.K. performed deep sequencing, M.H. constructed plasmids. H.Z. and L.T.J. supervised experiments. E.F. and L.T.J. wrote the manuscript with input from all authors.

**Competing interests:** The authors declare no competing interests.

**Corresponding author:** Correspondence should be addressed to Lucas T. Jae (jae@genzentrum.lmu.de).

**Extended Data Figure Legends:**

**Extended Data Figure 1 | CHOP and CHOP$^{Neon}$ protein levels in the context of different types of pharmacological stimulation. a**, Wild-type HAP1 cells were treated as indicated for 9 h and analyzed by immunoblotting. **b**, Schematic depicting the expected cellular activities of CCCP, TM and CDDO. **c**, CRISPR engineering of the *DDIT3* locus resulting in an endogenous in-frame fusion of CHOP with 3xFlag followed by mNeon as indicated. **d**, Pharmacological stimulation of wild-type HAP1 CHOP$^{Neon}$ cells for 9 h (TM and CDDO) or 16 h (CCCP) leads to induction of the CHOP$^{Neon}$ protein measured by flow cytometry (one representative of three independent experiments). **e**, Schematic depicting the generation of CHOP$^{Neon}$ cells and their interrogation in phenotypic genetic screening after exposure to cellular stress. Mutagenized cells were sorted based on mNeon intensity (Neon$^{lo}$ and Neon$^{hi}$ populations) and gene-trap mutations in these populations were analyzed by deep sequencing. **f**, Regulators of CHOP$^{Neon}$ in the genome-wide screen using CDDO. n = $1.90 \times 10^7$ interrogated single cells. Genes are colored as in Figs. 1a, b, dark grey denoting significant enrichment for mutations (two-sided Fisher's exact test, FDR-corrected *P*-value ($P_{adj}$) < 0.05). The two remaining EIF2α kinases GCN2 and PKR are additionally highlighted in black. **g**, HAP1 cells were exposed to sgRNAs targeting one of the four EIF2α kinases, pharmacologically stimulated for 9 h as indicated and assayed for CHOP induction by immunoblotting (one representative of two independent experiments). **h-m**, Common regulators of CHOP$^{Neon}$ in the genome-wide screens using CCCP, TM or CDDO. Data from Figs. 1a, b and (**f**), with statistical significance of mutation enrichment assessed and visualized as therein. Significant positive regulators ($P_{adj}$ < 0.05) with a mutation ratio < 0.25 (**h-j**) or negative regulators with a mutation ratio > 4 (**k-m**) that are shared across all three datasets are highlighted in red. ER, endoplasmic reticulum; LONP, LON protease 1; ΔΨ, mitochondrial membrane potential.

**Extended Data Figure 2 | Unique negative regulators of CHOP$^{Neon}$ across genetic screens. a-c,** Data from Figs. 1a, b and Extended Data Fig. 1f, with statistical significance of mutation enrichment assessed and visualized as therein. Genes that were identified as significant negative regulators (two-sided Fisher's exact test, $P_{adj}$ < 0.05) and had a mutation ratio > 4 in the query dataset, but neither of the other two datasets are highlighted in red: CCCP vs. TM & CDDO (**a**), TM vs. CDDO & CCCP (**b**), CDDO vs. CCCP & TM (**c**).

**Extended Data Figure 3 | Unique positive regulators of CHOP$^{Neon}$ across genetic screens. a-c,** Data from Figs. 1a, b and Extended Data Fig. 1f, with statistical significance of mutation enrichment assessed and visualized as therein. Genes that were identified as significant positive regulators (two-sided Fisher's exact test, $P_{adj}$ < 0.05) and had a mutation ratio < 0.25 in the query dataset, but neither of the other two datasets are highlighted in red: CCCP vs. TM & CDDO (**a**), TM vs. CDDO & CCCP (**b**), CDDO vs. CCCP & TM (**c**).

**Extended Data Figure 4 | Overview of positive and negative regulators of CHOP$^{Neon}$ following different drug treatments. a-c**, Data from Figs. 1a, b and Extended Data Fig. 1f, with statistical significance of mutation enrichment assessed and visualized as therein. For all datasets, significant positive regulators (two-sided Fisher's exact test, $P_{adj}$ < 0.05) with a mutation ratio < 0.25 (corresponding to an effect size of 4x or greater) are highlighted in blue, whereas significant negative regulators (two-sided Fisher's exact test, $P_{adj}$ < 0.05) with a mutation ratio > 4 are shown in yellow.

**Extended Data Figure 5 | Intersection of the most pronounced positive regulators of CHOP$^{Neon}$ across genetic screens and validation of DELE1 and HRI as mediators of**

**mitochondrial stress. a,** Data from Figs. 1a, b and Extended Data Fig. 1f, processed as therein, except that genes identified as highly significant positive regulators (two-sided Fisher's exact test, $P_{adj} < 10^{-5}$) with a mutation ratio < 0.25 in the CCCP dataset but neither the TM nor the CDDO dataset are highlighted in red. **b**, Venn diagram showing the results of stringent filtering of positive $CHOP^{Neon}$ regulators from (**a**; two-sided Fisher's exact test, $P_{adj} < 10^{-5}$ and mutation ratio < 0.25) as intersection between all three genetic screens performed in this study. **c**, HeLa, 293T cells, fibroblasts (BJEH), and keratinocytes (N/TERT-1) were exposed to sgRNAs directed against the specified genes and pharmacologically stimulated for 9-12 h prior to immunoblotting (one representative of n=2 (HeLa and 293T) or n=3 (BJEH and keratinocytes (N/TERT-1)) independent experiments). **d**, Clonal HAP1 knockout and stably reconstituted cells were treated as indicated (CCCP, TM, OM 9 h; CDDO, GTPP 11 h) and analyzed by immunoblotting. **e**, HAP1 $CHOP^{Neon}$ cells of the indicated genotypes were treated for 9 h (CCCP, TM, CDDO) or 12 h (GTPP) and analyzed by flow cytometry. Per genotype and treatment, the $CHOP^{Neon}$ signal was normalized to its DMSO control and statistical significance is indicated compared to identically treated wild-type cells (mean ± s.d. of n=3 independent experiments; one-way ANOVA with Dunnett's multiple comparisons correction). **f**, Wild-type, DELE1-deficient, and stably reconstituted HAP1 $CHOP^{Neon}$ cells were transduced with lentiviral constructs carrying a nontargeting control sgRNA or an sgRNA directed against LONP1. $CHOP^{Neon}$ levels were analyzed by flow cytometry. Per genotype, $CHOP^{Neon}$ fluorescence of sgLONP1-treated cells is depicted relative to its matching sgCTR-treated control (n=2 independent experiments). **g**, HeLa, 293T and HCT116 wild-type cells and cells transiently exposed to an sgRNA against HRI or DELE1 were stimulated with CCCP for 1 h and phosphorylation of EIF2α was analyzed by immunoblotting (one representative of two independent experiments). OM, oligomycin. sgCTR, non-targeting control sgRNA.

**Extended Data Figure 6 | DELE1 operates upstream of HRI, is cleaved and accumulates in the cytosol across different perturbations and cellular systems. a**, **b** HeLa wild-type, knockout and stably reconstituted cells were treated for 1 h (phospho-EIF2α) or 9 h (CHOP) with CCCP. Cells were analyzed by immunoblotting (**a**) and phospho-EIF2α levels were quantified relative to ACTB (**b**; mean ± s.d. of n=5 independent experiments; for each genotype, CCCP treatment was compared to DMSO using a paired two-tailed students *t*-test). **c**, **d**, Subcellular localization of HA-tagged DELE1 or $DELE1^{\Delta MTS}$ in HeLa cells analyzed by confocal microscopy. TRAP1 staining identifies mitochondria and nuclei were visualized with DAPI. **e**, Clonal DELE1 knockout $CHOP^{Neon}$ HAP1 cells were transiently transfected with full-length DELE1 ($DELE1^{FL}$) or truncation mutants lacking the first 101 ($DELE1^{\Delta MTS(N101)}$) or 115 ($DELE1^{\Delta MTS(N115)}$) amino acids (top) as indicated. Transfected cells were treated with CCCP or DMSO for 9 h and analyzed by flow cytometry as in Fig. 2a (mean ± s.d. of n=3 independent biological samples; two-way ANOVA with Tukey's multiple comparisons correction; one representative of 3 independent experiments). **f**, HeLa cells were transfected with DELE1-HA, treated with CCCP alone or CCCP + CHX as indicated, and analyzed for subcellular localization of DELE1. Mitochondria were stained with Mitotracker and nuclei were visualized using DAPI. **g**, CRISPR engineering of the *DELE1* locus in 293T cells (introducing a C-terminal in-frame fusion with a triple HA-tag), followed by treatment with CCCP or CCCP + CHX and analysis by immunoblotting (one representative of four independent experiments). **h**, HAP1 wild-type and HRI knockout cells were transfected with DELE1-HA and treated as indicated. The fate of the DELE1-HA protein was analyzed by immunoblotting (n=5 (HRI) or 2 (WT) biologically independent clones). **i, j**, HCT116 (**i**) and HAP1 (**j**) cells were transfected with DELE1-HA, treated with the specified compounds and analyzed for DELE1-HA cleavage and CHOP induction by immunoblotting (one representative of two independent experiments). **k**, Keratinocytes (N/TERT-1), $hTERT^{+}$

(BJEH) and primary fibroblasts were transduced with DELE1-HA, stimulated for 4 h as indicated and assayed by immunoblotting. **l**, Wild-type 293T and HAP1 cells were transfected with DELE1-HA and treated with CCCP for 4 h. Localization of DELE1-HA was analyzed as in Fig. 2d (one representative of two independent experiments). **m-o**, Cells from (**k**) stimulated as indicated for 4 h and localization of DELE1-HA and MFN2 were analyzed by confocal microscopy. TRAP1 stainings (**m**), Mitotracker (**n, o**), and DAPI (**o**) were used to visualize cellular substructures (one representative of two independent experiments). Scale bars: 10 µm.

**Extended Data Figure 7 | Processing of full-length DELE1 into S-DELE1 is mediated by catalytically active OMA1. a**, Data from Fig. 1a, with statistical significance of mutation enrichment assessed and visualized as therein (two-sided Fisher's exact test, $P_{adj} < 0.05$). Known mitochondrial proteases[44,45] are highlighted in red. **b**, Wild-type HAP1 cells and clonal OMA1 knockouts were transfected with DELE1-HA, treated and assayed by immunoblotting. **c**, HeLa cells of the stated genotypes were transfected with DELE1-HA, pretreated with the indicated protease inhibitors for 5 h, followed by the addition of CCCP for 2 h. The fates of DELE1, OMA1 and OPA1 were monitored by immunoblotting. **d**, Quantification of (**c**). The fraction of S-DELE1 (vs. L-DELE1) is indicated. Statistical significance was assessed using one-way ANOVA with Tukey's multiple comparisons correction as post hoc procedure, depicting significance relative to WT + CCCP (mean ± s.d. of n=3 independent experiments). **e**, HeLa cells transiently exposed to an sgRNA directed against OMA1 were co-transfected with the indicated cDNAs and cleavage of DELE1-FmN after 2 h of CCCP treatment was monitored by immunoblotting (one representative of two independent experiments). **f**, Workflow of *in organello* assay for DELE1 fate upon mitochondrial depolarization using mitochondria purified from wild-type or OMA1-deficient 293T cells transiently transfected with DELE1-HA. **g, h**, Purity analysis of isolated mitochondria using electron microscopy (**g**) and immunoblotting (**h**) (one representative of two independent experiments, each). For immunoblotting ca. 1% of the mitochondrial and 0.2% of the cytosolic fraction were used. Electron micrographs show high mitochondrial proportion and purity, only slight contaminations of membrane fragments or other cell organelles and the complete absence of intact cells within the mitochondrial suspensions. Scale bars equal 5 µm or 1 µm, respectively. **i-k**, Isolated mitochondria from (**g**, **h**) were treated *in vitro* with FCCP and analyzed for DELE1 processing. (**i**) Mitochondria build up a membrane potential that remains stable for one hour (demonstrated by constant low fluorescence). 500 nM FCCP was used to induce dissipation of the mitochondrial membrane potential, yielding an increase in fluorescence. (**j**) After 1h of FCCP treatment, mitochondria and supernatant were separated by centrifugation, protein levels in both compartments were analyzed by immunoblotting (long exposure for DELE1-HA is shown on top, short exposure below). (**k**) Amounts of S-DELE1 in the supernatants were quantified and compared to WT + DMSO using two-way ANOVA with Tukey's multiple comparisons correction. (**i**) and (**k**) depict mean ± s.d. of n=5 independent experiments. (**j**) shows one representative of n=5 independent experiments, of which purity analysis shown in (**g**) and (**h**) was performed for two independent experiments. Pepstat. A, Pepstatin A; o-Phen, o-Phenanthroline.

**Extended Data Figure 8 | DELE1 cleavage and subcellular redistribution following CCCP treatment depend on OMA1 but not OPA1. a-c**, HeLa cells were treated with sgRNAs directed against OPA1, stimulated and analyzed as indicated alongside wild-type HeLa cells by immunoblotting (**a**). Quantification of OPA1 levels (**b**) and DELE1 cleavage (**c**), compared to OPA1 levels and DELE1 cleavage observed upon CCCP treatment in wild-type cells. Statistical significance was assessed using one-way ANOVA with Tukey's multiple comparisons correction as post hoc procedure, depicting significance relative to WT (mean ± s.d. of n=4 biologically independent samples). **d**, HAP1 cells treated and analyzed as

in (**a**; one representative of two independent experiments). **e**, Data from Fig. 1a, with statistical significance of mutation enrichment assessed and visualized as therein (two-sided Fisher's exact test, $P_{adj} < 0.05$), highlighting OPA1 in red. **f**, HeLa cells treated with an sgRNA directed against OPA1, stimulated with CCCP and analyzed for DELE1 localization and OPA1 status alongside wild-type HeLa cells and OMA1 knockout cells. Arrowheads highlight OPA1-deficient cells. Scale bars: 10 μm; one representative of two independent experiments.

**Extended Data Figure 9 | Physical interaction between DELE1 and HRI. a**, 293T cells were co-transfected with StrepTagII-HA-HRI and the indicated Flag-mNeon-tagged cDNAs prior to stimulation with CCCP as indicated. Subsequently, cells were lysed, StrepTagII-containing protein complexes were immobilized on Streptactin beads and analyzed by immunoblotting alongside input lysate. **b**, A C-terminal in-frame fusion of a triple Flag-tag was introduced into the endogenous HRI locus of 293T cells using CRISPR. **c**, Quantification of Fig. 3b. Depicted is the relative abundance of the slowly migrating species of HRI (phosphorylated HRI) compared to the faster migrating band. Data were normalized to EV (black) and significance (compared to $DELE1^{FL}$ untreated, grey) was assessed using one-way ANOVA with Dunnett's multiple comparisons correction as post hoc procedure (mean ± s.d. of n=3 independent experiments). **d**, 293T cells were co-transfected with HRI-Flag and DELE1-HA and exposed to CCCP for the denoted amounts of time prior to immunoblotting. Electromobility shift of HRI upon activation is reversed by treatment of the lysates with alkaline phosphatase. **e**, 293T cells of the indicated genotypes were co-transfected with HRI-Flag and the specified HA-tagged constructs. After CCCP treatment, lysates were immobilized on anti-Flag beads and analyzed by immunoblotting alongside input (one representative of four independent experiments). **f**, Quantification of (**e**; mean ± s.d. of n=4 independent experiments; two-way ANOVA with Tukey's multiple comparisons correction). **g**, HeLa cells were transiently transfected with the indicated constructs, treated, and analyzed for subcellular localization of the transfected cDNAs by HA staining and confocal microscopy with cellular structures labelled as indicated. **h**, DELE1 mutants were transiently transfected into HeLa and 293T cells prior to exposure to CCCP for 2 h. DELE1-HA processing was monitored by immunoblotting. **i**, HeLa cells transfected as indicated and analyzed as in (**g**). **j**, 293T cells were co-transfected with HRI-Flag and the indicated StrepTagII-HA cDNAs. Subsequently, cells were lysed, StrepTagII-containing protein complexes were immobilized on Streptactin beads and analyzed by immunoblotting alongside input lysate. **k, l**, Clonal HAP1 DELE1 knockout cells were transiently transfected with the specified cDNAs alongside mCherry and induction of $CHOP^{Neon}$ was monitored by flow cytometry as in Fig. 2a. Per genotype, data were normalized to EV and statistical significance (compared to $DELE1^{\Delta MTS(N101)}$) was assessed using one-way ANOVA with Tukey's multiple comparisons correction (mean ± s.d. of n=4 independent experiments). **m**, Wild-type 293T cells were transiently transfected with HRI-Flag and the indicated HA-bearing cDNAs and processed as in (**e**; one representative of four independent experiments). **n**, DELE1-deficient $CHOP^{Neon}$ HAP1 cells were transiently transfected as indicated and analyzed by flow cytometry 32 h after transfection. Per genotype, data were normalized to EV (black) and statistical significance (compared to $DELE1^{\Delta MTS}$) was assessed using one-way ANOVA with Tukey's multiple comparisons correction as post hoc procedure (mean ± s.d. of n=3 independent experiments). **o**, Cell lysates from Fig. 3c were analyzed by Coomassie staining before (lysate) and after exposure to GFP-TRAP beads (GFP-IP). Scale bars: 10 μm.

**Extended Data Figure 10 | Effects of heme and mitochondrial membrane potential on the OMA1-DELE1-HRI pathway. a**, Schematic depiction of heme metabolism. **b**, Data from Fig. 1a, with statistical significance of mutation enrichment assessed and visualized as

therein (two-sided Fisher's exact test, $P_{adj} < 0.05$) and heme-related genes from (**a**) highlighted in red. **c**, Immunoprecipitation experiment as in Extended Data Fig. 9a in the presence of hemin during cell culture (20 μM for 12 h prior to lysis) and the immunoprecipitation (8 μM in lysis and wash buffers). HMOX1 is induced in response to increased heme levels (one representative of two independent experiments). **d**, Model of the pathway identified herein. Mitochondrial stress activates OMA1, which leads to cleavage of DELE1 and its subsequent cytosolic binding and activation of HRI, triggering the ISR. **e**, Wild-type HAP1 and HeLa cells treated with CCCP, with mitochondrial membrane potential visualized by TMRM using a live cell imaging system. H2B-GFP was transfected to stain nuclei. Scale bars: 100 μm. **f, g**, HAP1 $CHOP^{Neon}$ cells were stimulated as indicated. $CHOP^{Neon}$ levels and mitochondrial membrane potential were quantified by flow cytometry. Statistical significance is depicted relative to DMSO treated control cells (mean ± s.d. of n=3 independent experiments; one-way ANOVA with Tukey's multiple comparisons correction). **h**, HeLa cells were transfected with the indicated sgRNAs and mitochondrial membrane potential was quantified after 1 h of CCCP treatment by flow cytometry. TMRM signal was normalized to the non-targeting sgCTR + DMSO control and for CCCP-treated samples statistical significance was assessed relative to sgCTR + CCCP (mean ± s.d. of n=3 independent experiments; two-way ANOVA with Dunnett's multiple comparisons correction). **i**, Volcano plots of RNAseq analysis of the indicated samples. For every gene, expression fold change (FC) upon CCCP treatment (vs. DMSO-treatment, x-axis) is plotted against the *P*-value (DESeq2 two-tailed Wald test; y-axis). Genes with a significant differential expression ($P_{adj} < 10^{-12}$ (Benjamini-Hochberg); |log2 FC| > 1.5) are depicted in dark grey. ATF4/CHOP target genes (green)[39,40] and heat-shock proteins (red)[43] from Fig. 3e are highlighted (n=4 biologically independent samples per group).

**Extended Data Figure 11 | Cellular fitness and mitochondrial function in cells perturbed in the DELE1-HRI-eIF2α axis. a**, HAP1 cells were infected with lentivirus expressing TagRFP and indicated sgRNAs. A 1:1 mixture of infected and uninfected cells was treated for 48 h with 5 μM CCCP or DMSO and analyzed by flow cytometry. Abundance of $RFP^+$ sgRNA-containing cells following CCCP treatment was compared with the respective DMSO-treated sample bearing the same sgRNA and normalized to a non-targeting control sgRNA. Statistical significance is assessed compared to a second non-targeting control (sgCTR) using one-way ANOVA with Dunnett's multiple comparisons correction as post hoc procedure (mean ± s.d. of n=5 independent experiments). **b**, **c**, HAP1 cells of the indicated genotypes were treated as indicated for 48 h and cell survival was visualized using crystal violet (one representative of three independent experiments). **d-j,** HeLa wild-type and DELE1 knockout cells stably expressing the indicated cDNAs were subjected to different mitochondrial stressors and the oxygen consumption rate (OCR) was monitored. Within the same clonal background, no significant difference between DELE1-deficient and -proficient cells could be observed in non-mitochondrial oxygen consumption (**e**), basal respiration (**f**), maximal respiration (**g**), proton leak (**h**), ATP production (**i**) and spare respiratory capacity (**j**). Mean ± s.d. of n=4 independent culture wells from one representative of three independent experiments is shown. Statistical significance was assessed using one-way ANOVA with Tukey's multiple comparisons correction as post hoc procedure. Rot/AA, rotenone/antimycin A. **k, l**, Wild-type HAP1 cells, MFN2 knockouts and stably reconstituted cells were lentivirally transduced with a construct encoding TagRFP alongside a non-targeting control sgRNA, or an sgRNA directed against HRI (**k**) or DELE1 (**l**) and the fraction of $RFP^+$ cells was monitored over time. The abundance of sgDELE1 or sgHRI containing cells was normalized to non-targeting sgRNA and $t_0$ measurement (mean ± s.d. of n=3 biologically independent, separately infected and cultured wells per sgRNA and genotype; one-way ANOVA with Dunnett's multiple comparisons correction; one representative of two

independent experiments). **m**, SH-SY5Y cells exposed to the respective sgRNAs treated as in Extended Data Fig. 5c (one representative of four independent experiments). **n, o,** DELE1-HA processing and cellular localization in SH-SY5Y cells as in Extended Data Fig. 6k, o. MFN2-FmN served as a control (one representative of two independent experiments). Scale bars: 10 µm.

**Supplementary Table Information:**

**Supplementary Tables 1-3. Results of haploid genetic screens for CHOP$^{Neon}$ regulators using CCCP (Supplementary Table 1), tunicamycin (Supplementary Table 2) and CDDO (Supplementary Table 3).** Data were processed as described in the methods section. The columns are: gene symbol, mutations identified in the respective gene in CHOP$^{Neon}$-low cells, all other mutations identified in CHOP$^{Neon}$-low cells, mutations identified in the respective gene in CHOP$^{Neon}$-high cells, all other mutations identified in CHOP$^{Neon}$-high cells, *P*-value, FDR-corrected *P*-value[9]. n = $2.12 \times 10^7$ (Supplementary Table 1), $2.07 \times 10^7$ (Supplementary Table 2), or $1.90 \times 10^7$ (Supplementary Table 3) interrogated single cells.

**Supplementary Table 4. Oligonucleotides used in this study.**

**Supplementary Table 5. Antibodies used in this study.**
WB, Western Blot; FACS, fluorescence-activated cell sorting; IF, Immunofluorescence; IP, Immunoprecipitation.

**Supplementary Tables 6-10. Results of RNAseq analysis upon CCCP treatment: HAP1 wild-type cells (Supplementary Table 6), wild-type cells co-treated with ISRIB (Supplementary Table 7), HRI knockout cells (Supplementary Table 8), DELE1 knockout cells (Supplementary Table 9), and DELE1 knockout cells stably reconstituted with DELE1 (Supplementary Table 10).** Data were processed as described in the methods section (n=4 biologically independent samples per group). The columns are: gene symbol, mean of normalized counts for all samples (baseMean), log2 fold change (MLE): condition treated (CCCP) vs. untreated (DMSO), standard error: condition treated vs untreated, Wald statistic: condition treated vs untreated, Wald test *P*-value (two-tailed): condition treated vs. untreated, Benjamini-Hochberg adjusted *P*-value.

**Supplementary Figure Information:**

**Supplementary Figure 1. Uncropped blot source data.** All antibodies for one panel were probed on the same membrane, except for Ext. Data Fig. 1a where HSPD1 and ACTB were probed on the same membrane and CHOP on a different membrane, and for Fig. 3c where GST and GFP were probed on two different membranes. Cropping to achieve the final figure panel was performed in Adobe Illustrator or Photoshop.

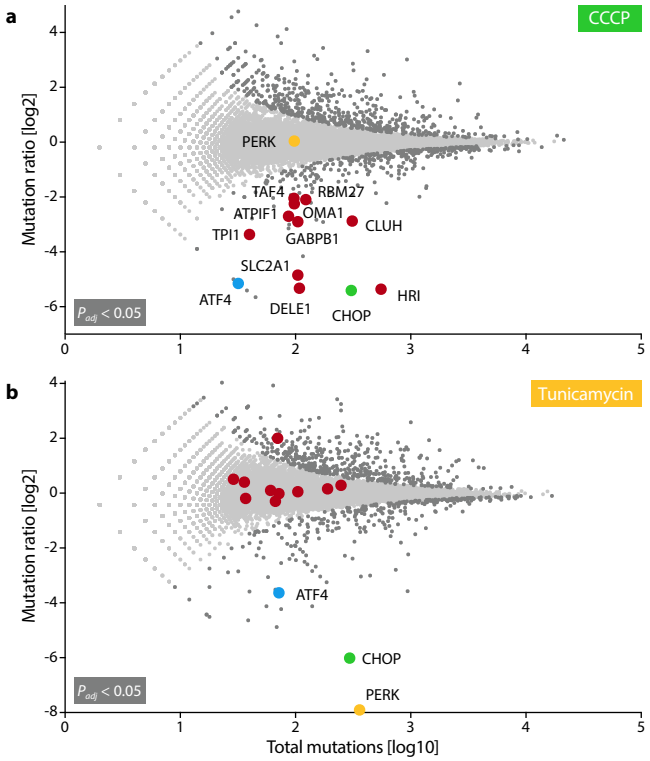
a
CCCP
Mutation ratio [log2]
PERK
TAF4
RBM27
ATPIF1
OMA1
CLUH
TPI1
GABPB1
SLC2A1
ATF4
DELE1
CHOP
HRI
$P_{adj}$ < 0.05
b
Tunicamycin
Mutation ratio [log2]
ATF4
CHOP
PERK
$P_{adj}$ < 0.05
Total mutations [log10]

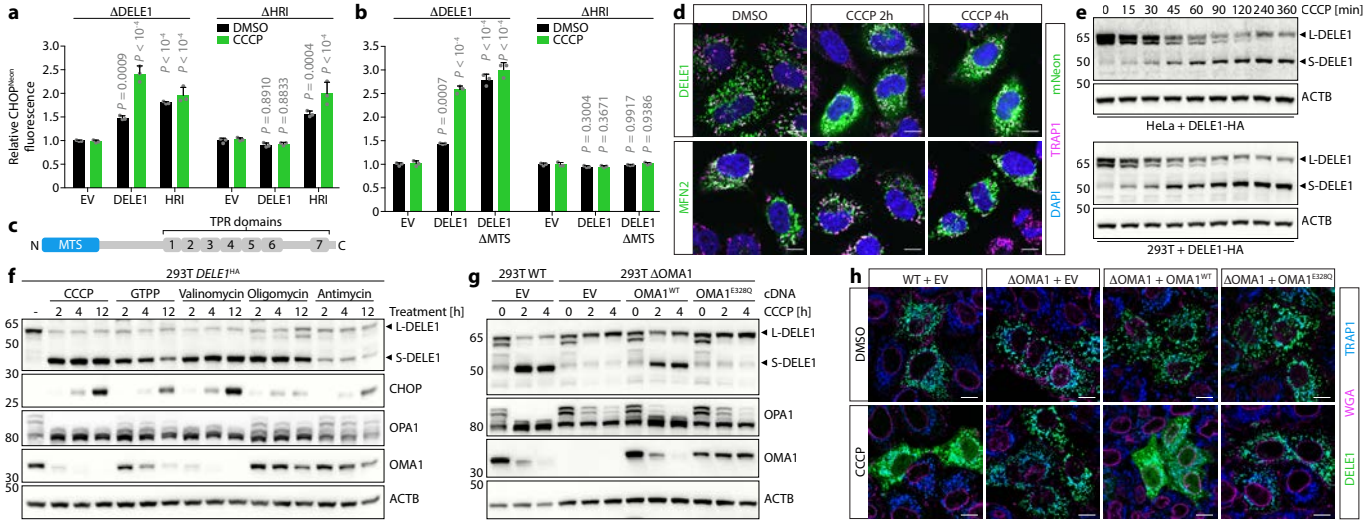
a
ΔDELE1
ΔHRI
DMSO
CCCP
Relative CHOP^Neon fluorescence
P = 0.0009
P < 10^-4
P < 10^-4
P < 10^-4
P = 0.8910
P = 0.8833
P = 0.0004
P < 10^-4
EV
DELE1
HRI
b
ΔDELE1
ΔHRI
DMSO
CCCP
P = 0.0007
P < 10^-4
P < 10^-4
P < 10^-4
P = 0.3004
P = 0.3671
P = 0.9917
P = 0.9386
EV
DELE1
DELE1 ΔMTS
c
TPR domains
N
MTS
1 2 3 4 5 6 7
C
d
DMSO
CCCP 2h
CCCP 4h
DELE1
MFN2
mNeon
TRAP1
DAPI
e
0 15 30 45 60 90 120 240 360 CCCP [min]
L-DELE1
S-DELE1
ACTB
HeLa + DELE1-HA
293T + DELE1-HA
f
293T DELE1^HA
CCCP
GTPP
Valinomycin
Oligomycin
Antimycin
Treatment [h]
L-DELE1
S-DELE1
CHOP
OPA1
OMA1
ACTB
g
293T WT
293T ΔOMA1
EV
OMA1^WT
OMA1^E328Q
cDNA
CCCP [h]
L-DELE1
S-DELE1
OPA1
OMA1
ACTB
h
WT + EV
ΔOMA1 + EV
ΔOMA1 + OMA1^WT
ΔOMA1 + OMA1^E328Q
DMSO
CCCP
TRAP1
WGA
DELE1

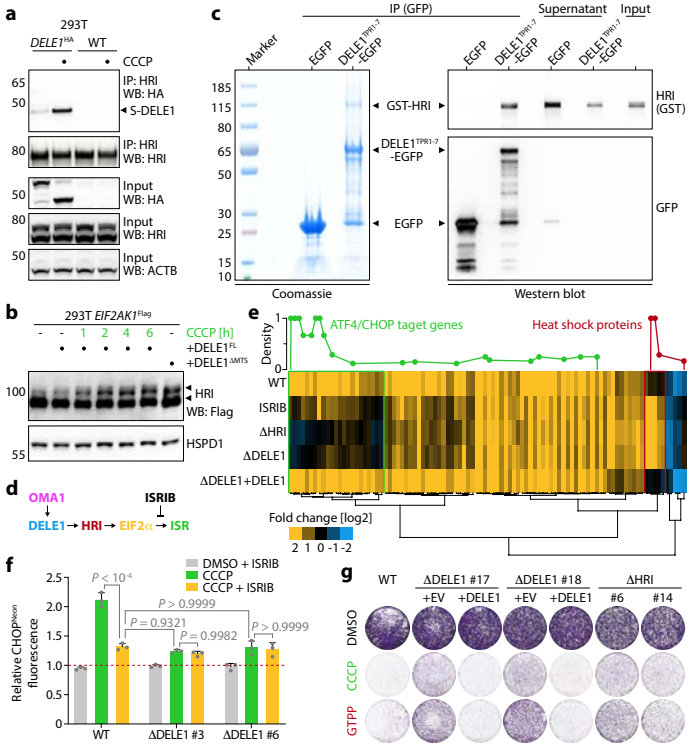
a
293T
DELE1HA
WT
CCCP
IP: HRI
WB: HA
S-DELE1
IP: HRI
WB: HRI
Input
WB: HA
Input
WB: HRI
Input
WB: ACTB
c
IP (GFP)
Supernatant
Input
Marker
EGFP
DELE1TPR1-7 -EGFP
GST-HRI
DELE1TPR1-7 -EGFP
EGFP
HRI (GST)
GFP
Coomassie
Western blot
b
293T EIF2AK1Flag
CCCP [h]
+DELE1FL
+DELE1ΔMTS
HRI
WB: Flag
HSPD1
e
ATF4/CHOP taget genes
Heat shock proteins
Density
WT
ISRIB
ΔHRI
ΔDELE1
ΔDELE1+DELE1
Fold change [log2]
d
OMA1
ISRIB
DELE1 → HRI → EIF2α → ISR
f
DMSO + ISRIB
CCCP
CCCP + ISRIB
Relative CHOPNeon fluorescence
P < 10-4
P > 0.9999
P = 0.9321
P = 0.9982
P > 0.9999
WT
ΔDELE1 #3
ΔDELE1 #6
g
WT
ΔDELE1 #17
ΔDELE1 #18
ΔHRI
+EV
+DELE1
+EV
+DELE1
#6
#14
DMSO
CCCP
GTPP